PROTEINS: Structure, Function, and Genetics 29:141–152 (1997)

Crystal Structures of the Methane Monooxygenase Hydroxylase From *Methylococcus capsulatus* (Bath): Implications for Substrate Gating and Component Interactions

Amy C. Rosenzweig,[1,3] Hans Brandstetter,[1,3] Douglas A. Whittington,[3] Pär Nordlund,[2] Stephen J. Lippard,[3]* and Christin A. Frederick[1]
[1]*Department of Biological Chemistry and Molecular Pharmacology, Harvard Medical School and Dana Farber Cancer Institute, Boston, Massachusetts*
[2]*Department of Molecular Biology, Stockholm University, S-10691, Stockholm, Sweden*
[3]*Department of Chemistry, Massachusetts Institute of Technology, Cambridge, Massachusetts*

ABSTRACT **The crystal structure of the nonheme iron-containing hydroxylase component of methane monooxygenase hydroxylase (MMOH) from *Methylococcus capsulatus* (Bath) has been solved in two crystal forms, one of which was refined to 1.7 Å resolution. The enzyme is composed of two copies each of three subunits ($\alpha_2\beta_2\gamma_2$), and all three subunits are almost completely α-helical, with the exception of two β hairpin structures in the α subunit. The active site of each α subunit contains one dinuclear iron center, housed in a four-helix bundle. The two iron atoms are octahedrally coordinated by 2 histidine and 4 glutamic acid residues as well as by a bridging hydroxide ion, a terminal water molecule, and at 4°C, a bridging acetate ion, which is replaced at −160°C with a bridging water molecule. Comparison of the results for two crystal forms demonstrates overall conservation and relative orientation of the domain structures. The most prominent structural difference identified between the two crystal forms is in an altered side chain conformation for Leu 110 at the active site cavity. We suggest that this residue serves as one component of a hydrophobic gate controlling access of substrates to and products from the active site. The leucine gate may be responsible for the effect of the B protein component on the reactivity of the reduced hydroxylase with dioxygen. A potential reductase binding site has been assigned based on an analysis of crystal packing in the two forms and corroborated by inhibition studies with a synthetic peptide corresponding to the proposed docking position. Proteins 29:141–152, 1997.** © **1997 Wiley-Liss, Inc.**

Key words: nonheme iron enzyme; dinuclear iron center; leucine gate; reductase binding site; protein crystallography

INTRODUCTION

Methanotrophic bacteria use methane as their sole source of carbon and energy. Deposited between anaerobic sediments containing methanogenic (methane producing) bacteria and the atmosphere, these organisms control the flux of methane so that only a fraction of the gas released by degradation of organic carbon reaches the atmosphere.[1] In the first step of their metabolic pathway, methanotrophs oxidize methane to methanol (Equation 1) via the methane

$$CH_4 + NADH + H^+ + O_2 \rightarrow CH_3OH + NAD^+ + H_2O \quad (1)$$

monooxygenase (MMO) enzyme system. The details of how MMO effects the chemically difficult transformation of methane to methanol have become the focus of intense research in recent years for several reasons. First, methane can serve as a fuel source and chemical feedstock. Although the world supply of natural gas is similar in magnitude to that of petroleum,[2] methane is used far less frequently as an energy source because most reserves are found in remote locations, rendering transport of the gas a major obstacle. Conversion of methane to a liquid

Abbreviations: MMO, methane monooxygenase; MMOH, methane monooxygenase hydroxylase; TCE, trichloroethylene; MIR, multiple isomorphous replacement; PIP, di-μ-iodobis(ethylenediamine)diplatinum(II); EMTS, sodium ethylmercurithiosalicylate; TAMM, tetrakis(acetoxymercuri)methane; rms, root-mean-square.

Contract grant sponsor: National Institute of General Medical Sciences; Contract grant numbers: GM48388 and GM32134; Contract grant sponsor: Swedish National Research Council.

Dr. Rosenzweig's present address is Department of Biochemistry, Molecular Biology, and Cell Biology, Northwestern University, Evanston IL 60208.
*Correspondence to: Dr. Stephen J. Lippard, Department of Chemistry, Massachusetts Institute of Technology, Cambridge, MA 02139; and Dr. Christin A. Frederick, Dept. of Biological Chemistry and Molecular Pharmacology, Harvard Medical School, Boston, MA 02115.

Received 21 January 1997; Accepted 15 May 1997

such as methanol would solve the transport problem, but at present there is no large-scale efficient process for the direct oxidation of methane to methanol with molecular oxygen.[3] An understanding of biological methane oxidation may lead to an improved industrial process. Second, MMO is remarkable for its ability to process a wide range of hydrocarbons of varying structure and functional groups, including trichloroethylene (TCE),[4–6] a widespread ground water pollutant that is toxic and potentially carcinogenic.[7] This property has led to the application of methanotrophs for bioremediation of land and water contaminated by oil spills and other pollutants. Finally, increasing atmospheric concentrations of methane contribute to greenhouse warming.[8]

The sMMO from *Methylococcus capsulatus* (Bath) consists of three proteins: a reductase (R, 38.6 kDa), a regulatory protein (B, 15.5 kDa), and a hydroxylase (H, 251 kDa).[9] All three proteins are required for enzyme activity. The reductase is an iron-sulfur protein containing one [2Fe–2S] cluster and 1 equiv of flavin adenine dinucleotide (FAD); it serves to transfer electrons one at a time to the hydroxylase. The regulatory protein is a small polypeptide with no metal or prosthetic groups and has been implicated in several roles, including the coupling of electron transfer by the reductase with hydroxylation of substrate (ref. 9 and G.T. Gassner and S.J. Lippard, unpublished results, 1997) and affecting the rate and regioselectivity of substrate oxidation.[10,11] The hydroxylase is the site of methane oxidation and is the key component of the enzyme system. It is a multimeric protein, comprising two copies each of three different subunits; the holoenzyme is $\alpha_2\beta_2\gamma_2$ (α, 60.6 kDa; β, 45 kDa; γ, 19.8 kDa). The hydroxylase belongs to a growing class of functionally diverse carboxylate-bridged diiron proteins, which includes hemerythrin, the R2 protein of ribonucleotide reductase, purple acid phosphatase,[12–14] rubrerythrin,[15] and stearoyl-acyl carrier protein (ACP) Δ^9-desaturase.[14,16]

The three-dimensional structure of the holohydroxylase from *M. capsulatus* (Bath) was solved at 2.2 Å resolution[17] and subsequently at 1.7 Å resolution.[18] Recently, the x-ray structure of the highly homologous hydroxylase from *Methylosinus trichosporium* OB3b was determined at 2.0 Å resolution.[19] In this paper, we present additional structural details about the fully refined *M. capsulatus* (Bath) enzyme and describe for the first time a second crystal form, a packing analysis, which identifies a potential site for reductase binding that was experimentally verified, and evidence for a leucine gate, which could control substrate access to and/or product egress from the catalytic diiron center at the active site.

RESULTS AND DISCUSSION

The Overall Structure

The molecular structure of the hydroxylase has been described briefly elsewhere.[17] The molecule is relatively flat with approximate dimensions of 60 × 100 × 120 Å, and the two αβγ protomers are related by a noncrystallographic twofold symmetry axis (Fig. 1). There is only a slight departure from twofold symmetry, the rms deviations for the Cα carbons being 0.20 Å and 0.29 Å for the α subunit, 0.29 Å and 0.31 Å for the β subunit, and 0.20 Å and 0.33 Å for the γ subunit. The two values refer to the first and second crystal forms, respectively. The overall larger deviations from local symmetry in crystal form II may be a consequence of its less symmetric packing interactions, described in more detail below. Each α subunit houses a dinuclear iron center, and the two diiron centers are 44.3 Å apart as measured from the midpoint between the two iron atoms. The dimer interface forms a large canyon, and there is an opening in the center of the molecule (Fig. 2). The association between the two protomers involves helices from the α and β subunits, with most of the contacts between the two β subunits. The γ subunit is not involved in the dimer interaction (Fig. 1).

Crystal Packing Interactions

In crystal form I, the hydroxylase molecules are stacked along the thin dimension (Fig. 3a). The tight molecular packing, which is consistent with the solvent content of 44%, renders both protomers in an approximately symmetrical crystal lattice environment. By contrast, the packing is less symmetric and consequently looser in crystal form II (Fig. 3b). The solvent content of crystal form II is 53%. Most of the interactions between molecules in the form I crystal lattice occur at the surface formed by the two α subunits and on the sides of the molecule, near the γ subunit. In both forms there is a large space between molecules in the region of the canyon formed at the dimer interface. The major intermolecular contacts involve the α and γ subunits in both crystal forms, since the β subunit is mostly buried by the dimer contact.

Two different crystal forms were reported for the *M. trichosporium* OB3b protein, both of which contain crystallographic twofold axes passing through the homodimeric molecules.[19] By contrast, in both crystal forms of the *M. capsulatus* (Bath) enzyme, the two halves of the dimer are related by noncrystallographic, local twofold axes. This asymmetry is further reflected by the results of a dithionite/mediator crystal soaking experiment to reduce the dinuclear nonheme iron centers from the Fe_2(III) resting state to the Fe_2(II), O_2-reactive state; in this experiment, only one protomer was reduced.[18]

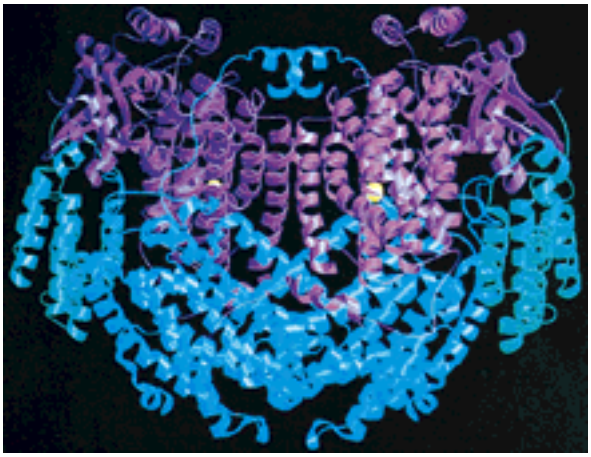

Fig. 1. The holohydroxylase. The α subunits are shown in *purple,* the β subunits are shown in *blue,* and the γ subunits are shown in *green.* The iron atoms are shown as *yellow* spheres. A noncrystallographic twofold axis runs vertically through the molecule in the plane of the page. This figure was generated by using the programs MOLSCRIPT[45] and RASTER3d.[46]

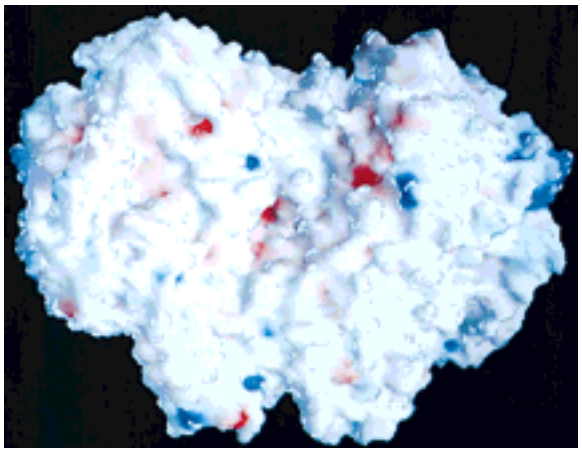

Fig. 2. Solvent-accessible solid surface of the hydroxylase. The color coding represents the electrostatic potential: *red* is negative and *blue* is positive. This figure was prepared by using the program GRASP.[47]

The Dinuclear Iron Center

The dinuclear iron centers are located within the α subunits, one in each half of the dimer. Both sites appear to be fully occupied. Four helices, αB, αC, αE, and αF, contribute the coordinating ligands. Helices αE and αF, which form part of the canyon, separate the iron atoms from the solvent. The diiron(III) cores in both the 4°C and −160°C structures are depicted in Figure 4 As described in more detail elsewhere,[17,18] each iron atom has octahedral coordination. One of the six ligands is the δ-nitrogen atom of a histidine residue, His147 to Fe1 and His246 to Fe2. By contrast, in hemerythrin, which contains a related diiron center, the histidine ϵ-nitrogen atoms are coordinated to the iron atoms.[20] In addition, there are four glutamic acid residues coordinated to the Fe atoms. Glu144 is semibridging, because the Fe2—O distance is too long for a normal coordinating distance (2.6 Å at 4°C and 2.5 Å at −160°C, average of both protomers in crystal form I). It formally contributes one oxygen atom to each iron atom. Fe1 is also coordinated by a monodentate carboxylate, Glu114, and a terminal water molecule, which is hydrogen bonded to the dangling oxygen atoms of Glu114 and Glu243. Fe2 is coordinated to two monodentate carboxylates, Glu209 and Glu243. There are also two exogenous bridging ligands, a hydroxide ion, consistent with optical, EXAFS,[21] and proton ENDOR[22] spectroscopic studies, and, in the 4°C structure, a bidentate bridging ligand assigned as an acetate ion since ammonium acetate was present in the crystallization buffer. This assignment is supported by recent ENDOR spectral investigations of acetate derivatives of the mixed-valent hydroxylase (J.-P. Willems, A.M. Valentine, S.J. Lippard, and B.M. Hoffman, unpublished results, 1997). In the −160°C structure, the acetate ligand is replaced by a monoatomic bridge, assigned as a water molecule. As a result of this substitution, the Fe···Fe distance is reduced from 3.4 Å at 4°C to 3.1 Å at −160°C. Recently, the diiron centers in chemically reduced[18] and DMSO-treated[23] forms of the hydroxylase crystals have been characterized, revealing that the exogenous ligand composition and carboxylate coordination modes can be readily altered. All of the iron-coordinating residues from the protein are conserved in the structures of the *M. capsulatus* and *M. trichosporium* OB3b enzymes.[19] The exogenous ligands are also the same except that, in the latter, the third bridging ligand was assigned as hydroxide rather than water and no acetate was present in the active site cavity.

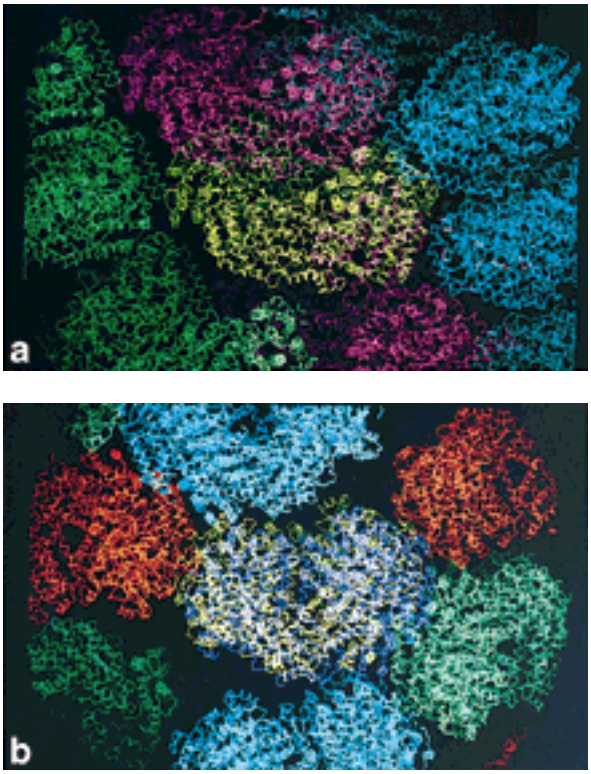

Fig. 3. **top:** Crystal packing interactions between one hydroxylase molecule of crystal form I shown in *yellow* and the surrounding molecules; different colors are chosen to correspond to symmetry generated molecules. **bottom:** Crystal packing interactions between one hydroxylase molecule of crystal form II shown in *yellow* and the surrounding molecules; different colors are chosen to correspond to symmetry-generated molecules. This figure was generated by using the program MAIN.[48]

Possible Substrate/Product Recognition Sites and the Leucine Gate

The diiron center in MMOH is situated in a hydrophobic cavity formed by the side chains of several adjacent amino acids (Fig. 5). The two iron atoms and the coordinating residues defining the active site are located on one surface of this cavity, designated as cavity 1 in Figure 6. The other sur-

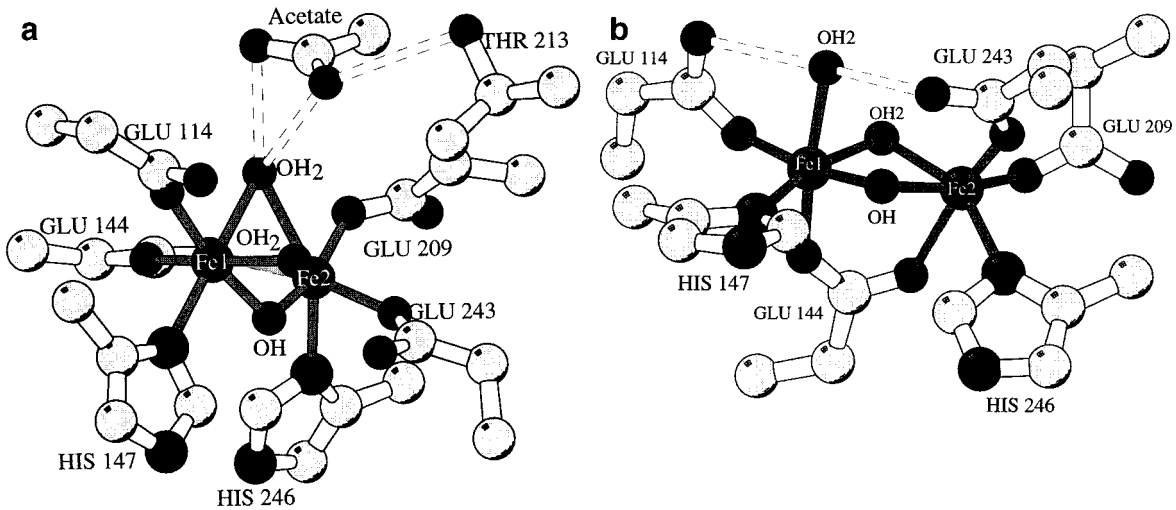

Fig. 4. Structure of the diiron center. **a:** The 2.2 Å resolution, 4°C structure. **b:** The 1.7 Å resolution, −160°C structure. This figure was generated by using the program MOLSCRIPT.[45]

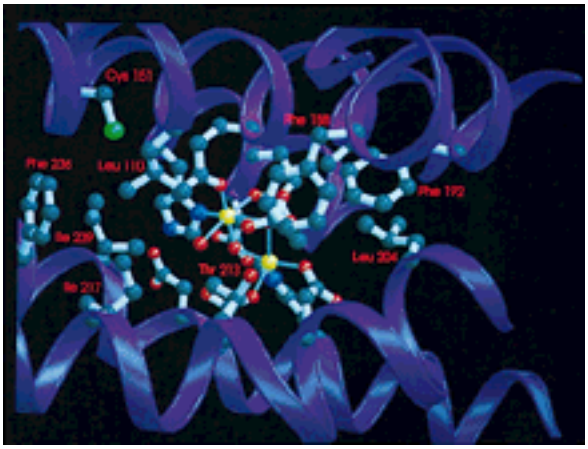

Fig. 5. The active site. The diiron center is located in a cavity lined with primarily hydrophobic residues. This figure was generated by using the programs MOLSCRIPT[45] and RASTER3d.[46]

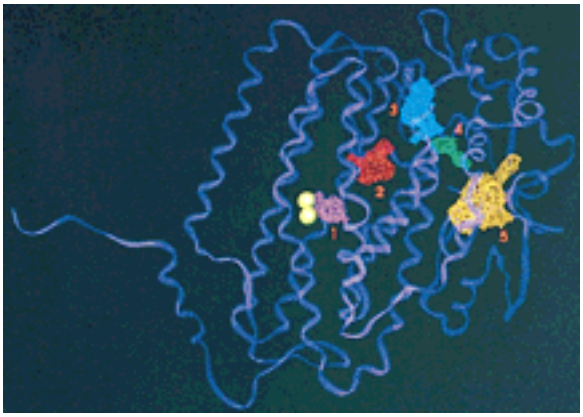

Fig. 6. Cavities present in the α subunit. This figure was generated by using the program O.[40]

faces of the cavity, with the exception of Thr213, contain hydrophobic side chains, including Ile217, Ile239, Phe236, Leu110, Phe188, Ala117, Phe192, Leu204, and Gly208. This type of environment, consisting of a metal binding site with a shell of hydrophilic coordinating residues surrounded by a second shell of hydrophobic residues, has been observed in a variety of metalloproteins.[24] The diiron center in hemerythrin is similarly located adjacent to such a hydrophobic cavity having the shape of an ellipse with major and minor axes of 4.8 and 3.5 Å, respectively (Fig. 7). Cavity 1 in MMOH can accommodate substrates ranging from small molecules such as methane and O_2 to portions of larger compounds like 2,2-diphenyl-1-methylcyclopropane,[25] and its dimensions are correspondingly larger, namely, 5.8 Å and 9.3 Å. There is a constriction near the middle of the long axis that partitions the cavity into two chambers of different size.

The MMOH α subunit contains a number of additional hydrophobic cavities (Fig. 6), identified by using the program VOIDOO[26] with a 1.2 Å radius probe. Most of these cavities are located between the active site and the second domain. The pocket closest to the diiron center (cavity 2) is completely hydrophobic, lined with residues Val105, Val106, Phe109, Leu110, Met184, Phe188, Leu216, Phe282, Val285, Leu286, and Leu289; it does not contain a single ordered water molecule. In crystal form II we find, consistently in both protomers, that Leu110 exhibits a different side chain conformation as compared with crystal form I (Fig. 8). As a consequence, cavities 1 and 2 are connected in form II. This connection is still too small (2.6 Å diameter) to allow passage of substrate, however. Figure 8 illustrates that additional movement of Leu110 (or Phe188) would afford a connection between the two cavities through which both substrates and products could pass. Since a

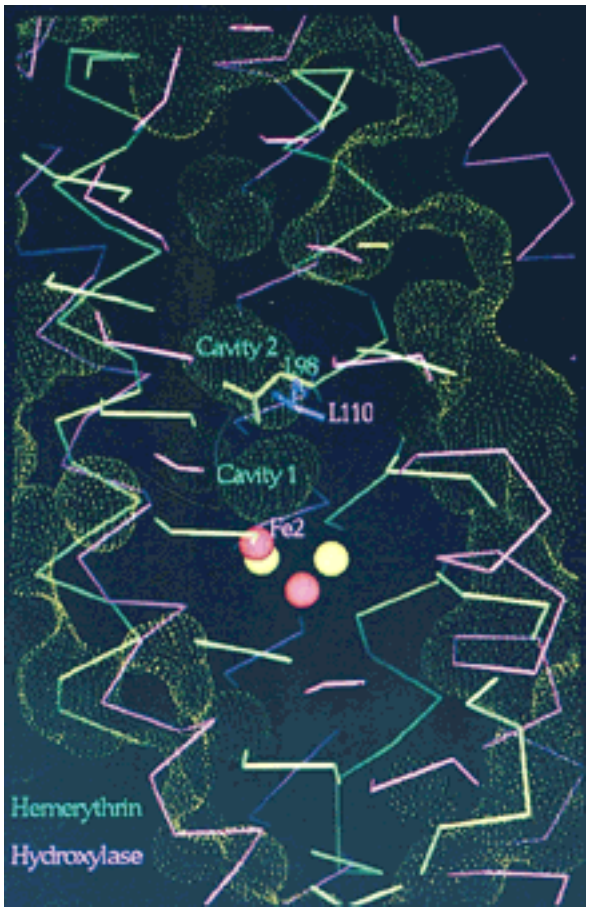

Fig. 7. Cavities present in hemerythrin (*green*) with hydroxylase (*purple*) superimposed. Superimposition was guided by optimizing the alignment of the four-helix bundle, conserving the hydroxylase helix polarities. This figure was generated by using the program MAIN.[48]

different crystal packing arrangement is sufficient to effect a side chain rearrangement for Leu110, we suggest that complex formation of the hydroxylase with protein B could induce just such a conformational shift in Leu110 to gate substrate recognition or access to, as well as product egress from, the active site. We have preliminary crystallographic data supporting the notion that cavity 2 may be functionally significant. In particular, a Xe atom, which has the same van der Waals radius as CH_4, was located in this cavity when crystals of MMOH were treated with a pressurized atmosphere of xenon (A.C. Rosenzweig, D.A. Whittington, C.A. Frederick, S.J. Lippard, Unpublished results, 1997). Finally, analysis of the previously published reduced MMOH structure[18] reveals that Leu110 shifts in an analogous manner in the reduced protomer. The conformation of the side chain in the oxidized protomer of this structure remains in the "closed" position.

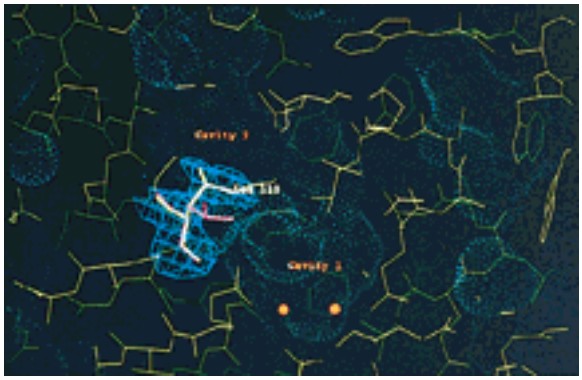

Fig. 8. The side chain of Leu 110 (*yellow*) as found in crystal form II with the corresponding electron density (*blue*). The conformation differs from that found in crystal form I (*purple*), thereby generating continously connecting cavities 1 and 2, represented by the *green* Conolly surface. This figure was generated by using the program MAIN.[48]

An analogous situation occurs in Hr, where two adjacent cavities 1 and 2 near the dinuclear center are separated by Leu98. Comparison of the structures reveals that Leu98 in Hr is exactly homologous to Leu110 in MMOH (Fig. 7). Recently, experimental evidence was obtained indicating that Leu98 functions as a substrate gate for reversible O_2 binding in hemerythrin (C.S. Farmer, J. Xiong, S. Arastu, D.M. Kurtz, Jr., Effects of site-directed mutagenesis on O_2 reactivity of hemerythrin and myohemerythrin, Personal communication, 1997). In particular, the L98A mutant exhibited increased autoxidation, whereas L98Y markedly decreased the dioxygen association and dissociation constants. These findings, together with our proposal for Leu110 in MMOH, suggest that leucine may serve the general function of gating substrates at hydrophobic cavities in dioxygen-utilizing metalloproteins.

Two additional large cavities (cavities 3 and 4 in Figure 6) lie just beyond cavity 2 and almost reach the surface of the protein. These two cavities are also lined primarily with hydrophobic side chains. It is conceivable that substrates could approach the active site through these pockets, that product could leave by this pathway, or that both substrates and product could access the active site via these pockets. Alternatively, the active site might be accessed by a shorter route, passing between helices E and F. In this scenario, Glu243 and the surface-located Glu240 would have to adopt altered conformations. Cavity 2 could then serve as a holding area for larger substrates. The distance from the diiron center to the surface through the E and F helices is only ~10–12 Å. Movement of Glu243 would be consistent with the observations that, in all datasets, the electron density representing this side chain is diffuse, suggest-

ing some conformational mobility. Perhaps a combination of both routes controls the $CH_4/O_2/CH_3OH$ transport pathway.

Component Interactions

No crystallographic data are currently available for the other two MMO components, the regulatory protein B and the reductase. Since protein B perturbs the EPR spectrum of the hydroxylase and alters the redox potential of its diiron center,[27–29] it may bind on the hydroxylase surface near the active site, as further suggested by chemical crosslinking to the α subunit.[28] In addition, MMOH/B binding affects both the rate and regioselectivity of substrate oxidation.[11,30] It is therefore likely that protein B causes a conformational change in the active site. The iron-coordinating helices αE and αF are exposed in the canyon formed between the two αβ pairs within the hydroxylase dimer and provide a good candidate for the regulatory protein binding site. Interaction between the two protein surfaces might indirectly affect the coordination environment of the two iron atoms, possibly in the form of carboxylate shifts analogous to those seen in the chemically reduced and DMSO-treated crystals.[23] The regulatory protein could also perturb the hydrogen bonding network that links His147 and His246 to Asp143, Asp242, Arg146, and Arg245 (Fig. 9).[17] Finally, the effects of component B binding might operate through conformational changes that open or close the Leu110 gate, altering the solvent composition of cavity 1 and affecting the properties of the dinuclear iron center. Since the hydroxylase binds 1.5–2 eq of regulatory protein,[10,28] a second molecule of this protein might bind in the canyon related by the noncrystallographic twofold symmetry axis.

The reductase does not affect the spectroscopic properties of the diiron center. It does physically interact with the hydroxylase, however, shifting the reduction potentials to favor two-electron reduction of the oxidized enzyme.[27,31] Chemical crosslinking of the reductase to the β subunit has been observed.[28]

As an independent line of investigating possible interaction sites of protein B and the reductase with the hydroxylase, we have used correlation analysis to examine packing interactions in both crystal forms. Our hypothesis was that helix–helix contacts between two MMOH molecules might mimic putative MMOH/R or MMOH/B binding motifs. As detailed in Materials and Methods, an 11-amino acid peptide of the reductase ($D^{24}EDVITAALRQ^{34}$) was identified as a good candidate for hydroxylase binding. To evaluate further this possibility, the peptide was synthesized and its binding to MMOH studied in a kinetic assay. The peptide inhibited MMO activity with an IC_{50} value of 500 μM, corresponding to a binding constant $K_d < 100$ μM. Its putative binding site is located on the second domain of the α subunit (Fig. 10). Significantly, superimposition of an homologous ferredoxin crystal structure (PDB entry 1FRD) onto the contact helix determined from the analysis resulted in a compatible packing interaction with no bad van der Waals contacts. According to this analysis the reductase should not bind in the canyon, but rather, on domain 2 of the α subunit. One immediate deduction from this docking experiment is that two reductase molecules can bind the hydroxylase without steric hindrance in a noncooperative manner. This conclusion is in excellent agreement with the results of recent calorimetric experiments (G.T. Gassner and S.J. Lippard, unpublished results, 1997). To be consistent with the crosslinking results mentioned above, we have to assume for this model that the reductase also contacts the N-terminal segment of the β subunit, which wraps around the second domain of the α subunit (Fig. 10). Crystal structures of complexes between the MMO components would more fully reveal the interactions among all three constituents.

MATERIALS AND METHODS

Protein Purification and Crystallization

The *M. capsulatus* (Bath) hydroxylase was purified as described elsewhere.[21] Crystallizations were carried out at 4°C by the vapor diffusion method with sitting drops in silanized 9-well glass spot plates. Crystalline needles and thin plates were obtained by using 10% PEG 4000, 25 mM Li_2SO_4, and 25 mM NH_4OAc in 25 mM MOPS, pH 7.0.[32] A macroseeding procedure was then used to grow larger, thicker crystals. Small seed crystals were washed and deposited into drops containing 15–35 mg/ml protein, 25 mM Li_2SO_4, 50 mM NH_4OAc, and 5% PEG 4000, which had been equilibrated versus a reservoir of 20% PEG 4000 for several days. Large crystals of typical dimensions $0.03 \times 0.15 \times 0.60$ mm^3 appeared within several weeks. The orthorhombic crystal have space group $P2_12_12_1$, with unit cell dimensions a = 62.6 Å, b = 110.1 Å, and c = 333.5 Å.

A second crystal form of the hydroxylase was obtained by the vapor diffusion method from a solution containing 5 μl of 7% PEG 8000, 20 mM MOPS pH 7.5, and 0.2 M $CaCl_2$ combined with 5 μl of 12.6 mg/ml concentrated protein solution (B:hydroxylase ratio 2:1). Repeated seeding experiments gave crystals with maximum dimensions of $0.5 \times 0.3 \times 0.08$ mm. Again, the crystals belong to orthorhombic space group $P2_12_12_1$ with unit cell dimensions a = 71.8 Å, b = 172.4 Å, and c = 221.9 Å. In both crystal forms there is one $\alpha_2\beta_2\gamma_2$ dimer of molecular weight 251 kDa in the asymmetric unit; crystal form II did not contain the B protein, and the crystals were reproduced in the absence of B. The Marresearch data sets and the 1.7 Å resolution Weissenberg data

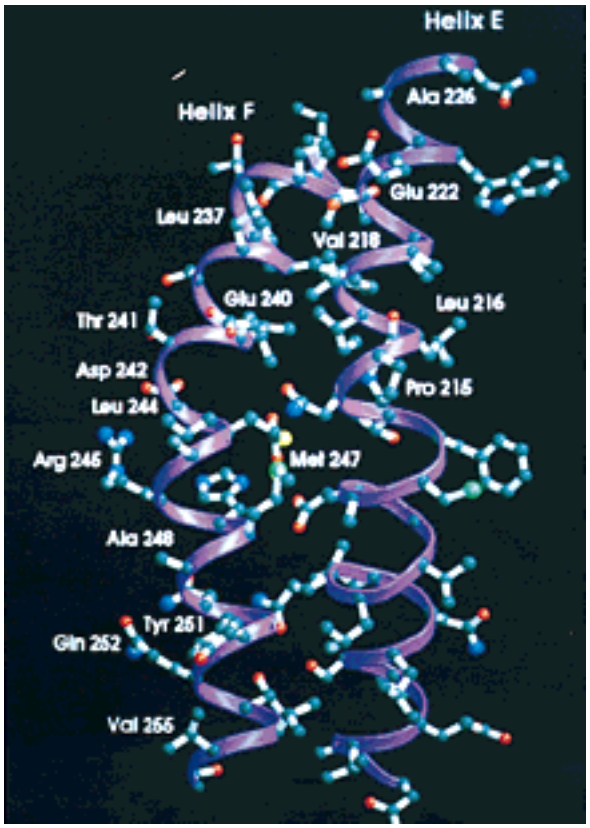

Fig. 9. Detailed view of helices αE and αF. The exposed residues are labeled. This figure was generated by using the programs MOLSCRIPT[45] and RASTER3d.[46]

were integrated by using the program DENZO[33] and scaled and merged by using either the programs ROTAVATA and AGROVATA in the CCP4 program package[34] or the program SCALEPACK.[33] The 2.2 Å resolution Weissenberg data were integrated by using the program WEIS,[35] followed by the standard CCP4 programs.

Heavy Atom Derivatives and Multiple Isomorphous Replacement (MIR) Phasing

An extensive search for isomorphous heavy atom derivatives of the form I hydroxylase crystals was conducted at the DFCI. Promising derivatives were recollected at SSRL at 3.0 Å or 3.7 Å resolution (Table I). Different combinations of the derivative datasets were refined together by using three different programs, HEAVY,[36] MLPHARE,[37] and REFINE.[34] The best phases as judged by the quality of the resulting MIR electron density map were obtained by using only SSRL derivative data. Three types of derivatives were used in the final phasing (Table I), and the mean figure of merit was 0.47 (MLPHARE) to 3.5 Å resolution.

Molecular Averaging, Model Building, and Refinement

Since the asymmetric unit consists of one $\alpha_2\beta_2\gamma_2$ dimer, the existence of a noncrystallographic twofold axis relating the two $\alpha\beta\gamma$ halves was investigated. The positions of the heavy atoms in the PIP and EMTS derivatives were used to locate the noncrystallographic twofold axis. A set of programs for molecular averaging, improvement of noncrystallographic symmetry, and molecular envelope definition written by T.A. Jones[38] was used for all averaging procedures. An initial molecular envelope was defined by using model coordinates from a skeletonized electron density map generated by using the program BONES.[39]

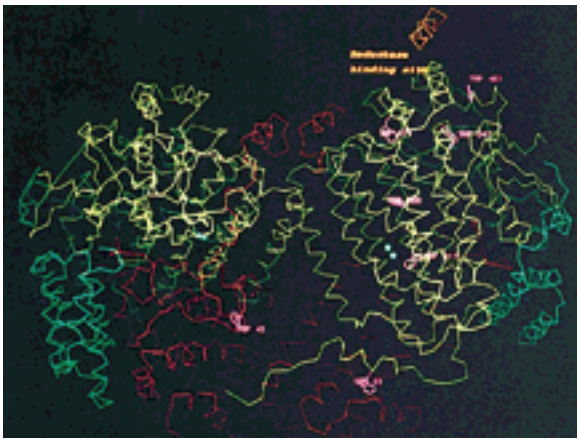

Fig. 10. Cα representation of the hydroxylase. The solvent-accessible tryptophan residues are highlighted in *purple.* The putative reductase contact helix, as localized by the packing analysis, is represented in *orange.* This figure was generated by using the program MAIN.[48]

TABLE I. Final Phasing Statistics

Compound	Resolution (Å)	Unique reflections	Completeness (%)	R_{merge} (%)*	Isomorphous difference (%)	Number of sites	Phasing power† (resolution)
Native‡	2.2	103,751	92	9.4			
Native −160°C	1.7	188,161	77	3.9			
PIP1	3.7	12,283	52	4.0	18.7	9	1.83 (4.3 Å)
PIP2	3.7	7,454	31	3.7	18.6	9	1.77 (3.8 Å)
TAMM1§	3.0	18,147	41	7.0	19.2	11	1.17 (3.5 Å)
TAMM2	3.0	18,279	41	7.9	19.8	9	1.32 (3.8 Å)
TAMM3	3.0	18,597	42	6.4	19.0	11	1.23 (3.5 Å)
TAMM4	3.0	15,215	34	6.7	19.1	11	1.32 (3.5 Å)
EMTS1	3.0	18,012	40	7.5	14.8	9	1.55 (3.5 Å)
EMTS2	3.0	27,471	62	6.3	15.0	9	1.78 (3.5 Å)
EMTS3	3.0	18,634	42	5.1	15.0	9	1.53 (3.5 Å)

PIP, di-μ-iodobis(ethylenediamine)diplatinum(II) nitrate; TAMM, tetrakis(acetoxymercuri)methane; EMTS, sodium ethylmercurithiosalicylate.

*$R_{merge} = \Sigma|I_{obs} - I_{avg}|/\Sigma I_{obs}$ where the summation is over all reflections.

†Phasing power = $rms(|F_H|_{calc})/rms(\epsilon)$ where $rms(|F_H|_{calc})$ is the root-mean-square calculated heavy atom structure factor and $rms(\epsilon)$ is the root-mean-square lack of closure error calculated by the program PHASE (CCP4 program package, SERC, Daresbury, U.K.).

‡All data collected at 4°C except where noted.

§For the TAMM derivative, one mercury atom was used for refinement of each site.

The modified density allowed the interpretation of several helices with a polyalanine model by using the program O.[40] At this stage phases were improved by combining the MIR phases with the refined model phases, and, in an iterative cycle of averaging, model building and refinement, the major parts of the electron density could be interpreted with a polyalanine model.

The sequence assignment was then accomplished starting with the iron-coordinating four-helix bundles, and by intepreting two mercury binding sites as the locations of the two cysteine residues near the diiron centers (Cys151 and Cys211). A total of 1570 water molecules were included into the final model, resulting in a final R factor of 18.3% (Table II). The coordinates for the 1.7 Å resolution structure have been deposited in the Protein Data Bank, entry number 1MTY.

Structure Determination and Refinement of Crystal Form II

The initial phasing problem was solved by Patterson search techniques using the dimeric molecular structure of crystal form I as the search model. All calculations were performed with XPLOR routines. The real space rotation function did not show a prominent peak, presumably due to the high internal molecular symmetry. The resulting list of possible orientations was then subjected to Patterson correlation refinement, which uniquely identified the correct molecular orientation. The correlation coefficient was 0.134 versus 0.022 of the next highest solution. A subsequent translation function verified the orthorhombic space group is $P2_12_12_1$, previously assigned from the systematic extinctions. The molecule was then refined as a rigid body, a restraint initially applied to the entire hydroxylase and subsequently by independent refinement of the subdomains. At that point the crystallographic R-factor had dropped to 32.3%. The electron density was inspected by using the program O and several side chain conformations were corrected. Most of these changes were caused by symmetry contacts. XPLOR was subsequently employed for restrained individual atom refinement (Table II).

Possible Contacts of a Reductase Helix With the Hydroxylase

Packing contacts in both MMOH crystal forms were analyzed in order to investigate the possible existence of surface areas on the hydroxylase that might mimic local surface patches on either the reductase or protein B suitable for complex formation with hydroxylase. Since the surface area of the hydroxylase is very large, it is possible that the enzyme contains such "self-recognition sites" and that these surface elements are involved in crystal lattice formation. Initially, all symmetry contacts in both crystal forms were examined on a computer graphics station using the program MAIN and restricted to contacts mediated by helices. All nonsecondary structure contacts were intentionally omitted, since such contacts can be induced by the partner molecule. Furthermore, as an additional selection criterion, we considered only helices with length >10 amino acids, corresponding to >3 helical turns. This restraint was applied for two reasons. First, it provided a means to check experimentally

TABLE II. Refinement Statistics

	RMS deviation from ideal geometry	
Distance (Å)	0.010	0.010
Bond angles (degrees)	1.5	1.5
Dihedral angles (degrees)	21.5	21.9

Resolution (Å)	R factor*	# Reflections
A. Crystal form I. 1.7 Å resolution, −160°C structure		
1.70–5.00	0.192	188123
1.70–1.76	0.245	14013
B. Crystal form II. 2.4 Å resolution, −160°C structure		
2.40–8.00	0.199	102861
2.40–2.51	0.259	8228

*The R factor is the crystallographic R factor

$$R = \frac{\Sigma \| F_{obs}(hkl) | - | F_{calc}(hkl) \|}{\Sigma | F_{obs}(hkl) |}$$

where the summation is over all reflections.

possible solutions by a peptide inhibition assay, since shorter peptides would be completely disordered when disengaged from their protein environment. Second, this length criterion represented a significance threshold. One major caveat with such an analysis is the obvious possibility that observed crystal contacts are enforced by other, large area interactions. We are aware of this limitation, but note that the crystallization of large enzymes differs considerably, and is often hindered, in the presence of small synthetic inhibitors. Based on this common experience we made the assumption that every extended crystal contact of three or more helical turns reflects an attractive interaction between the corresponding areas.

For crystal form I, only two helices of symmetry equivalent hydroxylase molecules fulfilled these criteria, designated X1h1 and X1h2, both of which are located on the γ subunit. For crystal form II four helices could be found, designated X2h1 through X2h4. For the six sequences a correlation analysis was pursued by using the AMPS program package.[41] With the application of a low gap penalty of 6.0, most of the helix sequences had to be split apart to match the target protein (B or reductase) over its entire length. Only two significant matches remained, X1h2 and X2h3. At this point we checked whether the secondary structure, calculated by the PHD method,[42,43] for these two reductase segments was predicted to be α-helical. This restriction eliminated one sequence, leaving only X2h3 as a possible candidate. In particular, the sequence of X2h3 (DKEEITASLYR) exhibited good homology with the reductase sequence D^{24}EDVITAALRQ^{34}. For the N-terminal part of the reductase, several homologous ferredoxin crystal structures are available. Inspection of several of those three-dimensional structures revealed that the segment D^{24}–R^{34} is indeed helical. In addition, upon superimposition of a (2Fe–2S) ferredoxin (PDB entry 1FRD) onto X2h3 we found a compatible binding interaction having no bad van der Waals contacts.

The 11mer D^{24}EDVITAALRQ^{34} was then synthesized and added to a standard MMO kinetic assay.[44] The peptide inhibited propylene oxide formation with an IC_{50} value of 500 μM, where IC_{50} is defined as the peptide concentration where 50% of the activity is inhibited. If we assume that the peptide competes only with the reductase, we get the relation in Equation 2 for the dissociation

$$K_d^{pept} = \alpha \left(\frac{1 + [R]}{K_d^R} \right)^{-1} \times IC_{50} = 0.11 \times IC_{50} \quad (2)$$

the peptide K_d^{pept} and IC_{50}, where $K_d^R = 1$ μM is the reductase/hydroxylase dissociation constant (G.T. Gassner and S.J. Lippard, unpublished results, 1997) and $[R] = 2.9$ μM, the free reductase concentration, which is determined by the experimental conditions. The factor $\alpha = 0.4$ corrects for the fact that the peptide will have $2^{-1/2} = 71\%$ of hydroxylase protomer sites occupied at half activity. According to crystallographic experience, structures of protein complexes with small ligands can be obtained if their dissociation constants are of the order of 200 μM.

In conclusion, we have identified a leucine residue which we propose to regulate substrate and/or product access to the hydrophobic pocket at the active site of sMMOH. This residue, which exhibits different side chain conformations in the two crystal forms and in the reduced hydroxylase, is in a position analogous to that of a leucine residue recently shown to be involved in gating dioxygen binding in Hr. In addition, a novel semi-empirical approach for the study of protein-protein interactions has been employed to locate a potential binding site for the reductase protein on the second domain of the alpha subunit. This binding site is consistent with the results of both peptide inhibition studies and docking experiments using a homologous ferredoxin domain. A more detailed understanding of substrate and component binding awaits crystallographic characterization of protein/protein complexes.

ACKNOWLEDGMENTS

This work was supported by grants from the National Institute of General Medical Sciences (GM48388 to S.J.L. and C.A.F. and GM32134 to S.J.L.) and the Swedish National Research Council (P.N.). A.C.R. was the recipient of a National Institute of General Medical Sciences postdoctoral fellowship,

and H.B. is grateful to the Alexander von Humboldt foundation for a Feodor-Lynen research fellowship. D.A.W. is an NIH Biotechnology Predoctoral Trainee. We thank P.M. Takahara, B.E. Earp, and A.C. Anderson for assistance with data collection and the staffs at SSRL and the Photon Factory for support.

REFERENCES

1. Higgins, I.J., Best, D.J., Hammond, R.C. New findings in methane-utilizing bacteria highlight their importance in the biosphere and their commercial potential. Nature 286:561–564, 1980.
2. Starr, C., Searl, M.F., Alpert, S. Energy sources: A realistic outlook. Science 256:981–987, 1992.
3. Periana, R.A., Taube, D.J., Evitt, E.R., Löffler, D.G., Wentrcek, P.R., Voss, G., Masuda, T. A mercury-catalyzed, high-yield system for the oxidation of methane to methanol. Science 259:340–343, 1993.
4. Colby, J., Stirling, D.I., Dalton, H. The soluble methane monooxygenase of *Methylococcus capsulatus* (Bath). Biochem. J. 165:395–402, 1977.
5. Green, J., Dalton, H. Substrate specificity of soluble methane monooxygenase. J. Biol. Chem. 264:17698–17703, 1989.
6. Fox, B.G., Borneman, J.G., Wackett, L.P., Lipscomb, J.D. Haloalkene oxidation by the soluble methane monooxygenase from *Methylosinus trichosporium* OB3b: Mechanistic and environmental implications. Biochemistry 29:6419–6427, 1990.
7. Ensley, B.D. Biochemical diversity of trichloroethylene metabolism. Annu. Rev. Microbiol. 45:283–299, 1991.
8. Chappellaz, J., Barnola, J.M., Raynaud, D., Korotkevich, Y.S., Lorius, C. Ice-core record of atmospheric methane over the past 160,000 years. Nature 345:127–131, 1990.
9. Colby, J., Dalton, H. Resolution of the methane monooxygenase of *Methylococcus capsulatus* (Bath) into three components. Biochem. J. 171:461–468, 1978.
10. Liu, K.E., Valentine, A.M., Wang, D., Huynh, B.H., Edmondson, D.E., Salifoglou, A., Lippard, S.J. Kinetic and spectroscopic characterization of intermediates and component interactions in reactions of methane monooxygenase from *Methylococcus capsulatus* (Bath). J. Am. Chem. Soc. 117: 10174–10185, 1995.
11. Froland, W.A., Andersson, K.K., Lee, S.-K., Liu, Y., Lipscomb, J.D. Methane monooxygenase component B and reductase alter the regioselectivity of the hydroxylase component-catalyzed reaction. J. Biol. Chem. 267:17588–17597, 1992.
12. Que Jr., L., True, A.E. Dinuclear iron- and manganese oxo sites in biology. Prog. Inorg. Chem. 38:97–200, 1990.
13. Vincent, J.B., Olivier-Lilley, G.L., Averill, B.A. Proteins containing oxo-bridged dinuclear iron centers: A bioinorganic perspective. Chem. Rev. 90:1447–1467, 1990.
14. Nordlund, P., Eklund, H. Di-iron-carboxylate proteins. Curr. Opin. Struct. Biol. 5:758–766, 1995.
15. deMare, F., Kurtz Jr., D.M., Nordlund, P. The structure of *Desulfovibrio vulgaris* rubrerythrin reveals a unique combination of rubredoxin-like FeS_4 and ferritin-like diiron domains. Nature Struct. Biol. 3:539–546, 1996.
16. Fox, B.G., Shanklin, J., Somerville, C., Münck, E. Stearoyl-acyl carrier protein Δ9 desaturase from *Ricinus communis* is a diiron-oxo protein. Proc. Natl. Acad. Sci. U.S.A. 90:2486–2490, 1993.
17. Rosenzweig, A.C., Frederick, C.A., Lippard, S.J., Nordlund, P. Crystal structure of a bacterial non-haem iron hydroxylase that catalyses the biological oxidation of methane. Nature 366:537–543, 1993.
18. Rosenzweig, A.C., Nordlund, P., Takahara, P.M., Frederick, C.A., Lippard, S.J. Geometry of the soluble methane monooxygenase catalytic diiron center in two oxidation states. Chem. Biol. 2:409–418, 1995.
19. Elango, N., Radhakrishnan, R., Froland, W.A., Wallar, B.J., Earhart, C.A., Lipscomb, J.D., Ohlendorf, D.H. Crystal structure of the hydroxylase component of methane monooxygenase from *Methylosinus trichosporium* OB3b. Protein Sci. 6:556–568, 1997.
20. Sheriff, S., Hendrickson, W.A., Smith, J.L. Structure of myohemerythrin in the azidomet state at 1.7/1.3 Å resolution. J. Mol. Biol. 197:273–296, 1987.
21. DeWitt, J.G., Bentsen, J.G., Rosenzweig, A.C., Hedman, B., Green, J., Pilkington, S., Papaefthymiou, G.C., Dalton, H., Hodgson, K.O., Lippard, S.J. X-ray absorption, Mössbauer, and EPR studies of the dinuclear iron center in the hydroxylase component of methane monooxygenase. J. Am. Chem. Soc. 113:9219–9235, 1991.
22. DeRose, V., Liu, K.E., Lippard, S.J., Hoffman, B. Proton ENDOR identification of bridging hydroxide ligands in mixed-valent diiron centers of proteins: methane monooxygenase and semimet azidohemerythrin. J. Am. Chem. Soc. 115:6440–6441, 1993.
23. Rosenzweig, A.C., Frederick, C.A., Lippard, S.J. Carboxylate shifts in the active site of methane monooxygenase. In: "Microbial Growth on C_1 Compounds: Proceedings of the Eighth International Symposium." Lidstrom, M.E., Tabita, F.R. (eds.). Dordrecht: Kluwer Academic Publishers, 1996: 141–149.
24. Yamashita, M.M., Wesson, L., Eisenman, G., Eisenberg, D. Where metal ions bind in proteins. Proc. Natl. Acad. Sci. U.S.A. 87:5648–5652, 1990.
25. Liu, K.E., Johnson, C.C., Newcomb, M., Lippard, S.J. Radical clock studies and kinetic isotope effect studies of the hydroxylation of hydrocarbons by methane monooxygenase. J. Am. Chem. Soc. 115:939–947, 1993.
26. Kleywegt, G.J., Jones, T.A. Detection, delineation, measurement and display of cavities in macromolecular structures. Acta Crystallogr. D50:178–185, 1994.
27. Liu, K.E., Lippard, S.J. Redox properties of the hydroxylase component of methane monooxygenase from *Methylococcus capsulatus* (Bath). J. Biol. Chem. 266:12836–12839, 24859, 1991.
28. Fox, B.G., Liu, Y., Dege, J.E., Lipscomb, J.D. Complex formation between the protein components of methane monooxygenase from *Methylosinus trichosporium* OB3b. J. Biol. Chem. 266:540–550, 1991.
29. Paulsen, K.E., Liu, Y., Fox, B.G., Lipscomb, J.D., Münck, E., Stankovich, M.T. Oxidation-reduction potentials of the methane monooxygenase hydroxylase component from *Methylosinus trichosporium* OB3b. Biochemistry 33:713–722, 1994.
30. Liu, K.E., Feig, A.L., Goldberg, D.P., Watton, S.P., Lippard, S.J. Methane monooxygenase: models and mechanism. In: "The Activation of Dioxygen and Homogeneous Catalytic Oxidation." Barton, D.H.R., Martell, A.E., Sawyer, D., (eds.). New York: Plenum, 1993:301–320.
31. Wallar, B.J., Lipscomb, J.D. Dioxygen activation by enzymes containing binuclear non-heme iron clusters. Chem. Rev. 96:2625–2657, 1996.
32. Rosenzweig, A.C., Frederick, C.A., Lippard, S.J. Crystallization and preliminary X-ray analysis of the methane monooxygenase hydroxylase protein from *Methylococcus capsulatus* (Bath). J. Mol. Biol. 227:283–285, 1992.
33. Otwinowski, Z. Data collection and processing. In: "Proceedings of the CCP4 Study Weekend." Warrington, UK: Daresbury Laboratory, 1993:56–62.
34. Collaborative Computational Project, Number 4. The CCP4 suite: Programs for protein crystallography. Acta Crystallogr. D50:760–763, 1994.
35. Higashi, T. The processing of diffraction data taken on a screenless Weissenberg camera for macromolecular crystallography. J. Appl. Crystallogr. 22:9–18, 1989.
36. Terwillinger, T.C., Eisenberg, D. Unbiased three-dimensional refinement of heavy-atom parameters by correlation of origin-removed Patterson functions. Acta Crystallogr. A39:813–817, 1983.

37. Otwinowski, Z. MLPHARE, CCP4 Proc. 80–88. Warrington, UK: Daresbury Laboratory, 1991.
38. Jones, T.A. a, yaap, asap, @#*? A set of averaging programs. In: "Molecular Replacement." Dodson, E.J., Glover, S., Wolf, W. (eds.). Warrington, UK: SERC Daresbury Laboratory, 1992:91–105.
39. Kleywegt, G.J., Jones, T.A. Halloween . . . masks and bones. In: "From First Map to Final Model." Bailey, S., Hubbard, R., Waller, D. (eds.). Warrington, UK: SERC Daresbury Laboratory, 1994:59–66.
40. Jones, T.A., Zou, J.-Y., Cowan, S.W., Kjeldgaard, M. Improved methods for building protein models in electron density maps and location of errors in these models. Acta Crystallogr. A47:110–119, 1991.
41. Barton, G.J. Protein multiple sequence alignment and flexible pattern matching. Methods Enzymol. 183:403–428, 1990.
42. Rost, B., Sander, C. Prediction of protein structure at better than 70% accuracy. J. Mol. Biol. 232:584–599, 1993.
43. Rost, B. PHD: Predicting one-dimensional protein structure by profile based neural networks. Methods Enzymol. 266:525–539, 1996.
44. Green, J., Dalton, H. Steady-state kinetic analysis of soluble methane monooxygenase from *Methylococcus capsulatus* (Bath). Biochem. J. 236:155–162, 1986.
45. Kraulis, P.J. MOLSCRIPT: A program to produce detailed and schematic plots of protein structures. J. Appl. Crystallogr. 24:946–950, 1991.
46. Merritt, E.A., Murphy, M.E.P. Raster3d Version 2.0: A program for photorealistic molecular graphics. Acta Crystallogr. D50:869–873, 1994.
47. Nicholls, A., Sharp, K.A., Honig, B. Protein folding and association: Insights from the interfacial and thermodynamic properties of hydrocarbons. Proteins 11:281–296, 1991.
48. Turk, D. Weiterentwicklung eines Programmes für Molekulgraphik und Elektronendichte-Manipulation und seine Anwendung auf verschiedene Protein Strukturaufklarungen. Ph.D. thesis, Technische Universität München. 1992.